Optics Communications 370 (2016) 140–144

Contents lists available at ScienceDirect

Optics Communications

journal homepage: www.elsevier.com/locate/optcom

Engineering near-field focusing of a microsphere lens with pupil masks

Bing Yan, Liyang Yue, Zengbo Wang *

School of Electronic Engineering, Bangor University, Bangor LL57 1UT, United Kingdom

ARTICLE INFO

Article history:
Received 4 January 2016
Received in revised form
17 February 2016
Accepted 2 March 2016

Keywords:
Microsphere
Super-resolution
Pupil mask
Diffraction limit
Near-field

ABSTRACT

Recent researches have shown small dielectric microspheres can perform as super-resolution lens to break optical diffraction limit for super-resolution applications. In this paper, we show for the first time that by combining a microsphere lens with a pupil mask, it is possible to precisely control the focusing properties of the lens, including the focusing spot size and focal length. Generally, the pupil mask can significantly reduce the spot size which means an improved resolution. The work is important for advancing microsphere-based super-resolution technologies, including fabrication and imaging.

1. Introduction

The diffraction limit of light focusing was discovered by Ernst Abbe [1]. This fundamental rule restrained the performance of conventional optical instruments to a resolution of roughly $\lambda/2$ in far-field in free space, where λ is the wavelength of incident light. Breaking diffraction limit and developing super-resolution technologies are constant themes in optical researches. One solution is near-field optics, which explores the optical phenomena occurring at subwavelength distance from scattering objects and often collecting information in evanescent wave at the boundary of two different media. Near-field scanning optical microscopy (NSOM), for example, has been developed to enhance the resolution by replacing lens with a tiny tip [2]. Nevertheless, the slow processing speed and the surface dependence limit its utility. Superlens and hyperlens, which were developed under the umbrella of Pendry's perfect lens concept, use metal and artificially engineered metamaterials to gain super-resolution at given optical wavelength. Their resolution is fundamentally limited by the material loss in metals [3–7]. Recently, it was discovered that microsphere can generate super-resolution focusing beyond diffraction limit, a phenomena known as 'photonic nanojet' [8–12]. This has led to the development of an exciting super-resolution imaging technique 'microsphere nanoscopy' by the present authors [13,14]. Different samples have been directly imaged in sub-wavelength resolution and real time without labeling, including both non-biological (nano devices, structures and materials) and biological (subcellular details, viruses) samples [15–17]. Besides our work, a notable advancement on the 'microsphere nanoscopy' technique is obtained by Darafsheh et al. who studied confocal mode imaging with microsphere superlens. Higher contrast super-resolution images have been achieved in their study due to the ability of confocal microscopy to reject out-of-focus lights [18]. Besides imaging, the microsphere lens has also been widely used for other applications, including for example nanofabrication and ultrahigh density data storage [19–22].

Ability to precisely control of focusing properties is highly desired for microsphere-based technologies. Despite in theory the best focusing can be obtained via controlling particle size, its refractive index with respect to surrounding medium and incident wavelength, in reality these conditions could be difficult to meet since desired microspheres may not be commercially available. It is therefore highly desirable to develop a new technique that can control the near-field focusing of a microsphere lens in a flexible and easy-to-implement way. In this paper, we propose to use pupil mask to achieve such controllability. It shall be noted we are dealing with near-field problems here, in which the focus is located very close to particle surface and evanescent wave components could be involved. This demands a full wave numerical simulation to include both propagating and evanescent wave modes. In contrast to this, previous researches on pupil mask assisted optical super-resolution were often focusing on far-field problems where no evanescent waves will be involved and simplified formulations can be used. Paeder et al. studied the effect of annular amplitude and phase masks on far-field microlenses [23]. Plenty of similar literature can be found in this regards, with applications in photolithography [24], data storage and confocal scanning microscopy [25,26] etc.

* Corresponding author.
E-mail address: z.wang@bangor.ac.uk (Z. Wang).

http://dx.doi.org/10.1016/j.optcom.2016.03.008

2. Simulation method

To describe the optical properties of small sphere, Mie theory plays a significant role over a century [27]. Many of the basic phenomena of microsphere focusing can be interpreted by this theory. However, focusing properties of small particle with pupil mask cannot be tackled by Mie theory and we seek to solve the problem with full wave simulation approaches. Several numerical calculation methods may be suitable for such propose, which includes for example the multiple multi-pole (MMP) [28] technique, discrete dipole approximation (DDA) [29] and pure numerical methods such as finite element method (FEM) [30], finite difference time domain (FDTD) technique [31], and Finite Integral Technique (FIT) [32]. The FIT technique, proposed by Weiland, provides a universal spatial discretization scheme, applicable to various electromagnetic problems, ranging from static field calculations to high frequency applications in time or frequency domain. Unlike most numerical methods, FIT discretizes Maxwell's equation in an integral form rather than the differential ones. In the case of Cartesian grids, the FIT formulation can be rewritten in time domain to yield standard FDTD methods. While in the case of triangular grids, the FIT has tight links with FEM methods formulated in Whitney forms [30]. In this paper, a commercial FIT software package (CST MICROWAVE STIDIO) was used. For better accuracy on simulation results, we have chosen to use triangular grids thus a FEM-like method in simulation, which are naturally conformal to the circular boundary of a sphere. The particle was discretized by tetrahedral meshes at a mesh density of $\lambda/4$, where λ is incident wavelength. The incident wave is a linearly polarized plane wave with electric vector polarized along the x-axis. The desired linear equation system solver accuracy in terms of the relative residual norm was set as 10^{-6}, which enforce a termination criterion for the solver. The retardation effect and contributions from all necessary orders of partial waves dipole, quadruple, etc. are inheritably considered in our modeling. Due to limitation of computation resources, the studied particle diameter was limited to 3 μm and below.

3. Results and discussions

Fig. 1 shows the schematics and corresponding electric intensity field distribution for (a, b) no-mask and (c, d) with mask

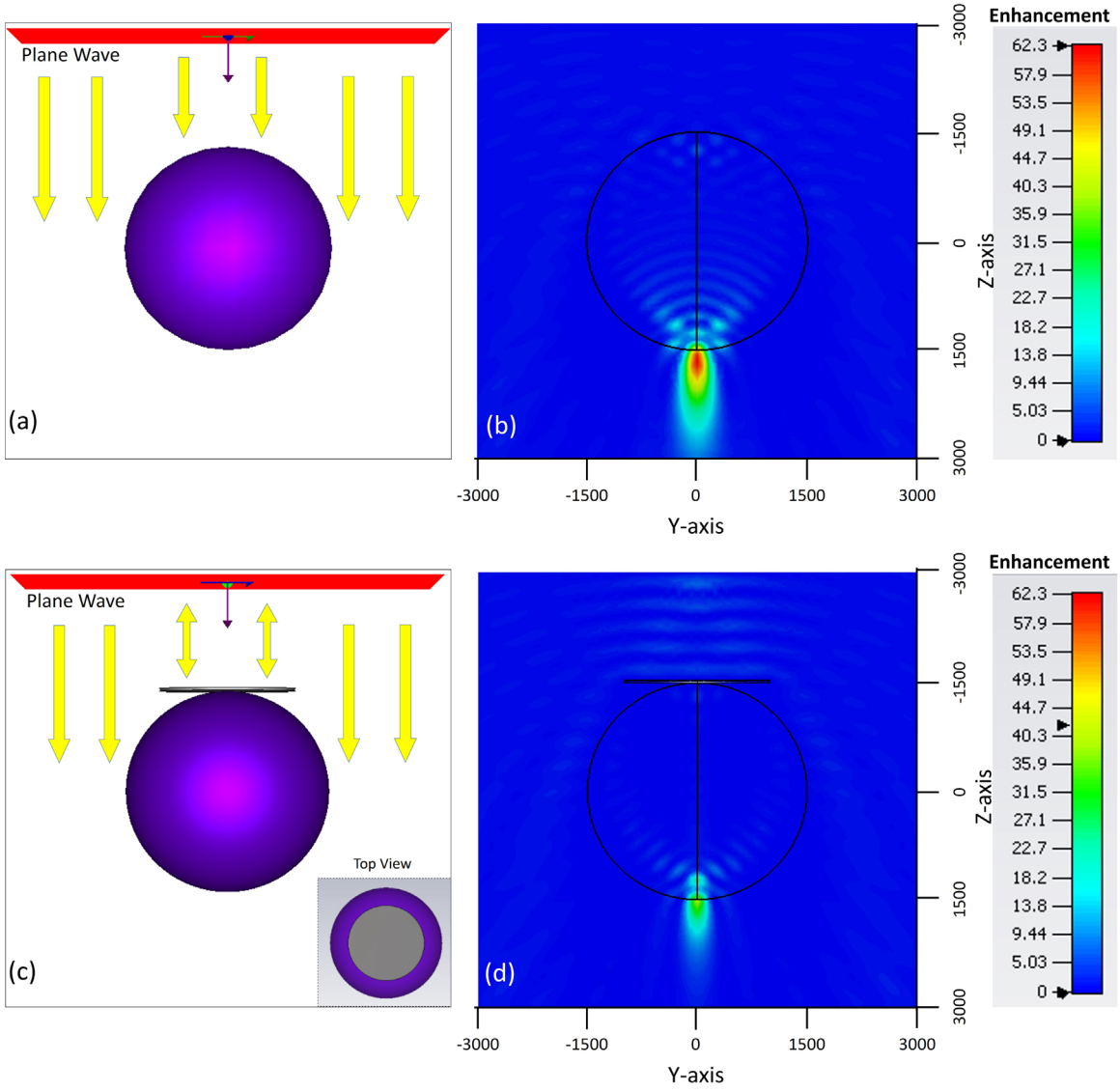

Fig. 1. Schematic diagrams and $|E|^2$ intensity field distributions for two microsphere systems. (a,b) single microsphere, (c,d) proposed microsphere with pupil mask system. Parameters: wavelength 600 nm, microsphere diameter 3 μm, and (c) with mask diameter 2 μm, refractive index (RI) of microsphere is 1.46 and mask material PEC).

case. The particle diameter was 3 μm in both cases. The pupil mask is a circular disk positioned right on top of the particle, with diameter 2 μm. Apart from particle and mask size parameters, other parameters were kept fixed in this research: refractive index of microsphere = 1.46 (SiO_2); background medium refractive index = 1 (air); incident wavelength = 600 nm, *x*-polarized, propagates along *z*-axis; pupil mask material = PEC (perfect electric conductor) which provides 100% blocking of incident light. It shall be noted that the optical resolution (Full Width of Half Maximum – FWHM value of minimum spot size) were measured using electric intensity field distributions ($|E|^2$) in *YZ* cross-sectional planes. This is because near-field focusing of microsphere lenses is generally elongated along incident polarization direction (*x*-axis) and minimum spot size (i.e. best resolution) is found on the *Y*-direction [33]. Unlike far-field lenses, near-field microsphere lens could generate internal focus inside the microsphere as well. Here we skipped analysis of such internal focuses but chose to use the exterior highest intensity position as resolution measurement position. This is because all existing demonstrated microsphere super-resolution applications are relying on the fields outside of microspheres. However, we believe new applications based on internal focusing fields will be developed in the future. Comparing Fig. 1(b) with (d), one can clearly see that with mask the focus spot has become smaller in both *y* and *z* directions. This means an improved lateral and axial resolution have been simultaneously achieved by the mask. This is an important finding of present study.

Fig. 2(a) shows 1D intensity field profiles along z axis for a 3 μm microsphere coupled with pupil masks, whose diameter varies from zero (no mask) to 3 μm (same as particle diameter). There are two intensity peaks, one inside and the other outside of particle. The external peak dominants over the internal peak when the mask size is smaller than particle size. It is interesting to note that, when mask size equals to particle size, the light is not fully blocked but still got a weak focusing due to light bending effects occurring in micro domains [34] which cannot be understood using ray optics. A clear tendency in the figure is that the external peak amplitude decreases quickly with mask size and meanwhile its focus position moves closer to the particle, leading to a shortened focal length. The internal peak, however, has shown much

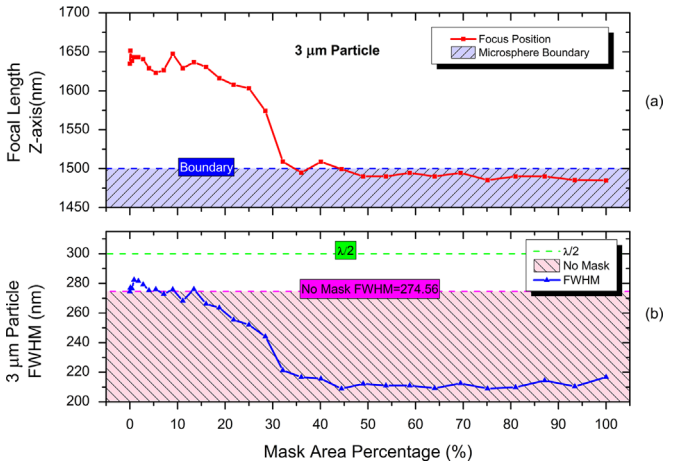

Fig. 3. Corresponding (a) focal length and (b) focus resolution (FWHM of focus spot) at external peak location as a function of mask area size, derived from Fig. 2 for 3 μm – diameter microspore lens coupled with varying size pupil masks.

less influenced by the mask; its amplitudes drops much slowly and its location remains almost unchanged. It should be noted the increased spatial resolution of marked microspheres was accompanied by the decreasing of focal intensity. Fig. 2(b) plots the corresponding intensity profile along the *y*-axis across external focus position. The resolution is measured using the FWHM size of each profile curve in the plot.

For the ease of comparison, we retrieved focal length and resolution data for the 3 μm particle from Fig. 2 and graphed them in Fig. 3 as a function of MAP (Masked Area Percentage of particle cross-section), which is defined as:

$$\mathrm{MAP} = \frac{\pi \times r^2}{\pi \times R^2} \times 100\% \tag{1}$$

where *r* is mask radius and *R* is particle radius. A higher MAP value means a larger sized mask. As shown in Fig. 3, at zero MAP (no mask), the focal length is about 1635 nm for the 3 μm microsphere. The focus is outside of sphere since it is larger than the

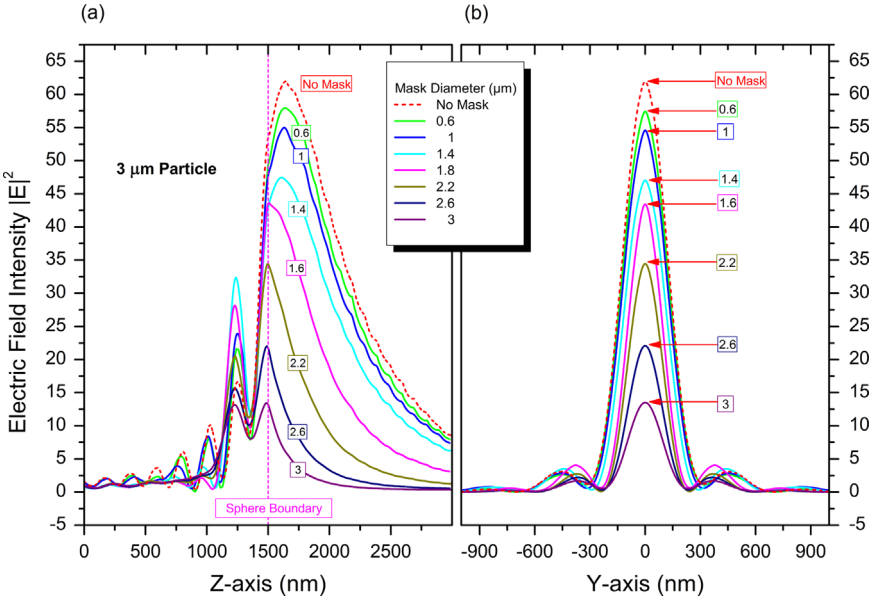

Fig. 2. (a) $|E|^2$ intensity field distribution along propagation axis *z* across 3 μm – diameter microsphere center, with varying pupil mask diameter from 0 to 3 μm (b) corresponding focus field profile along *Y*-axis which measures focusing resolution in exterior zones of the microsphere, the internal focusing was neglected in this study.

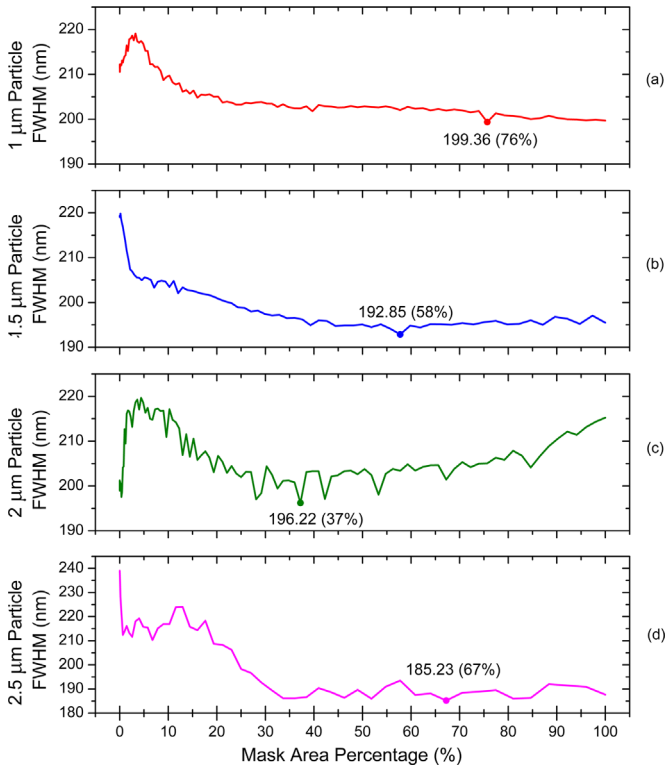

Fig. 4. Focusing resolution as a function of mask area percentage (MAP) for smaller diameter microsphere lenses: (a) 1.0 μm, (b) 1.5 μm, (c) 2.0 μm and (d) 2.5 μm.

particle radius of 1500 nm. Between 0% and 25% MAP, the focal length decreases slowly with small oscillations, but remains greater than the particle radius. Between 25% MAP and 35% MAP, however, the focal length decreases significantly faster, dropping from about 1600 nm to about 1500 nm. When MAP is above 35%, the focus position is relatively steady which remains close to the particle bottom surface, moving from outside to inside of the particle with less than 25 nm variations. At 100% MAP, the main focus is located inside the particle, about 15 nm away from the boundary. These results confirm the flexibility of using pupil mask to precisely control the focus position in optical near-fields, movable from outside particle zone to internal particle zone.

Fig. 3(b) shows corresponding resolution curve measured as a function of MAP at focus positions outside of particle. Note this curve is sitting below the classical diffraction limit curves ($\lambda/2$ as shown in the figure) which means the focuses are in super-resolution and beyond the diffraction limit. The resolution curve evolves in a way similar to the focal length curve in Fig. 3(a). At zero MAP (no mask), the focus FWHM size is about 274.56 nm ($=\lambda/2.19$). For MAP smaller than about 12%, the resolution show small oscillations but keep approximately at same size as no mask case. As MAP increases over 12%, the focus spot size drops quickly, reaching a minimum of 208.93 nm ($=\lambda/2.87$) at 44% MAP. This is the best resolution we can achieve for the discussed system, which is 76% smaller than the resolution for the reference case (no-mask). At higher MAP, the resolution is slightly lower and is oscillating around 220 nm ($=\lambda/2.73$). The small oscillations in both curves are not caused by numerical accuracy in simulation, but by multi-orders Mie resonances nature in the micro-sized particles; such oscillations are expected to be reduced in larger sized particles [27]. Due to limitation of computing resources, we would not be able to investigate such problem at present, but will look into it in the future when resources become available.

For smaller diameter microspheres, the pupil mask can produce similar super-resolution enhancement effect. Fig. 4 shows calculated resolution curve as a function of MAP for microsphere lenses with diameter (a) 1.0 μm, (b) 1.5 μm, (c) 2.0 μm and (d) 2.5 μm. Due to Mie-type resonances occurring in wavelength-scale microspheres, the resolution curves are in different evolution profiles, with ripples resulting from the coupling of different spatial field modes inside a sphere. However, a general tendency can be drawn for most particles: as mask size increases, the resolution tends to increases. This happens for particle sizes 1.0, 1.5 and 2.5 μm. However, the 2.0 μm particle seems slightly different, possibly due to the excitation of internal modes. Nevertheless, all studied particles have shown improved resolutions when the pupil mask was used. The corresponding optimized resolution data was retrieved from Figs. 3 and 4 and results were summarized in Table 1. As it can be seen, the best optimized resolution is 199.36 nm ($=\lambda/3$) for 1 μm particle, 192.85 nm ($=\lambda/3.11$) for 1.5 μm particle, 196.22 nm ($\lambda=/3.05$) for 2 μm particle and 185.23 nm ($=\lambda/3.24$) for 2.5 μm particle and 208.93 ($=\lambda/2.87$) for 3 μm particle, respectively. These optimized resolutions are well beyond the classical $\lambda/2$ diffraction limit and most of them have even exceeded the solid immersion resolution limit of $\lambda/2n=\lambda/2.97$ ($n=1.46$). The enhanced super-resolution gained through pupil mask is quite significant and we believe such effect will pay a big role in advancing all microsphere-based super-resolution techniques. In reality, the proposed pupil mask could be realized by projecting a millimeter scale mask through demagnification effect commonly used in photolithography [35].

4. Conclusions

In summary, we have shown that by using circular pupil mask and varying its size, it is possible to precisely tune the focal point of a microsphere lens in near-field zones from external zone to internal body of the microsphere, and meanwhile improve its focusing lateral resolution by more than 30% to close to 80%, leading to an optimized resolution hugely surpassing the classical diffraction limit. The work provides a new freedom in controlling super-resolution focusing of microsphere lens and is expected to play a big role in the future of microsphere-based super-resolution techniques.

Table 1
Best resolution for microspheres with pupil mask.

Microsphere diameter (μm)	Optimized MAP for best resolution (%)	Best resolution	Resolution improvement over no-mask case (%)
1	76	199.36 nm ($=\lambda/3.00$)	94
1.5	58	192.85 nm ($=\lambda/3.11$)	88
2	37	196.22 nm ($=\lambda/3.05$)	99
2.5	67	185.23 nm ($=\lambda/3.24$)	77
3	44	208.93 nm ($=\lambda/2.87$)	76

Acknowledgments

The authors would thank funding supports from Sêr Cymru National Research Networking Advanced Engineering and Materials, UK (Projects NRNF66 and NRN113).

References

[1] E. Abbe, Schultzes Arc. f Mikr. Anat. 9 (1873) 413–468.
[2] R.C. Dunn, Near-field scanning optical microscopy, Chem. Rev. 99 (1999) 2891.
[3] N. Fang, et al., Sub–diffraction-limited optical imaging with a silver superlens, Science 308 (2005) 534–537.
[4] Z. Liu, et al., Far-field optical superlens, Nano Lett. 7 (2007) 403–408.
[5] X. Zhang, et al., Superlenses to overcome the diffraction limit, Nat. Mater. 7 (2008) 435–441.
[6] Z. Liu, et al., Far-field optical hyperlens magnifying sub-diffraction-limited objects, Science 315 (2007) 1686.
[7] J.B. Pendry, Negative refraction makes a perfect lens, Phys. Rev. Lett. 85 (2000) 3966.
[8] Z. Chen, A. Taflove, V. Backman, Opt. Express 12 (2004) 1214–1220.
[9] A. Heifetz, S.C. Kong, A.V. Sahakian, A. Taflove, V. Backman, J. Comput. Theor. Nanosci. 6 (2009) 1979–1992.
[10] Y.E. Geints, A.A. Zemlyanov, E.K. Panina, J. Opt. Soc. Am. B 29 (2012) 758–762.
[11] X. Li, Z. Chen, A. Taflove, V. Backman, Opt. Express 13 (2005) 526–533.
[12] P. Ferrand, J. Wenger, A. Devilez, M. Pianta, B. Stout, N. Bonod, E. Popov, H. Rigneault, Opt. Express 16 (2008) 6930–6940.
[13] Z. Wang, W. Guo, L. Li, B. Luk'yanchuk, A. Khan, Z. Liu, Z. Chen, M. Hong, Nat. Commun. 2 (2011) 218.
[14] H. Guo, Y. Han, X. Weng, Y. Zhao, G. Sui, Y. Wang, S. Zhuang, Opt. Express 21 (2013) 2434–2443.
[15] S. Lee, L. Li, Y. Ben-Aryeh, Z. Wang, W. Guo, J. Opt. 15 (2013) 125710.
[16] L. Li, W. Guo, Y. Yan, S. Lee, T. Wang, Light: Sci. Appl. 2 (2013) e104.
[17] A. Darafsheh, C. Guardiola, A. Palovcak, J.C. Finlay, A. Cárabe, Opt. Lett. 40 (2015) 5–8.
[18] A. Darafsheh, N.I. Limberopoulos, J.S. Derov, D.E. Walker Jr., V.N. Astratov, Appl. Phys. Lett. 104 (2014) 061117.
[19] Z. Wang, N. Joseph, L. Li, B.S. Luk'yanchuk, Proc. Inst. Mech. Eng. C 224 (2010) 1113–1127.
[20] E. McLeod, C.B. Arnold, Nat. Nanotech. 3 (2008) 413–417.
[21] W. Wu, A. Katsnelson, O.G. Memis, H. Mohseni, Nanotechnology 18 (2007) 485302.
[22] S.-C. Kong, A.V. Sahakian, A. Heifetz, A. Taflove, V. Backman, Appl. Phys. Lett. 92 (2008) 211102.
[23] V. Paeder, T. Scharf, P. Ruffieux, H.P. Herzig, R. Voelkel, K. Weible, J. EOS-Rapid Commun. 2 (2007).
[24] N. Yao, Z. Lai, L. Fang, C. Wang, Q. Feng, Z. Zhao, X. Luo, Opt. Express 19 (2011) 15982–15989.
[25] M. Martınez-Corral, P. Andres, C.J. Zapata-Rodrıguez, M. Kowalczyk, Opt. Commun. 165 (1999) 267–278.
[26] G. Yang, Opt. Commun. 159 (1999) 19–22.
[27] G. Mie, Ann. Phys. 25 (1908) 377–445.
[28] C. Hafner, The Generalized Multipole Technique for Computational Electrodynamics, Artech House, Boston, 1990.
[29] W.H. Yang, G.C. Schatz, R.P. Vanduyne, J. Chem. Phys. 103 (1995) 869–875.
[30] J. Jin, The Finite Element Method in Electromagnetics, Wiley, New York, 2002.
[31] A. Taflove, Computational Electrodynamics: The Finite-Difference Time-Domain Method, Artech House, Boston, 2005.
[32] T. Weiland, Int. J. Numer. Model. 9 (1996) 295–319.
[33] Z. Wang, Y. Zhou, B. S. Luk'yanchuk, arXiv:1304.4139v2, 2013.
[34] C. Sheng, H. Liu, Y. Wang, S.N. Zhu, D.A. Genov, Nat. Photon. 7 (2013) 902–906.
[35] M. Rothschild, T.M. Bloomstein, N. Efremow, T.H. Fedynyshyn, M. Fritze, I. Pottebaum, M. Switkes, MRS Bull. 30 (2005) 942–946.